SANDIA REPORT
SAND2024-15221
Printed November 2024

Sandia National Laboratories

Integrating Atmospheric Specifications into Seismoacoustic Event Localization

Clinton Koch, Fransiska Dannemann Dugick

Prepared by
Sandia National Laboratories
Albuquerque, New Mexico
87185 and Livermore,
California 94550

Issued by Sandia National Laboratories, operated for the United States Department of Energy by National Technology & Engineering Solutions of Sandia, LLC.

Available to DOE and DOE contractors from
U.S. Department of Energy
Office of Scientific and Technical Information
P.O. Box 62
Oak Ridge, TN 37831

Telephone: (865) 576-8401
Facsimile: (865) 576-5728
E-Mail: reports@osti.gov
Online ordering: http://www.osti.gov/scitech

Available to the public from
U.S. Department of Commerce
National Technical Information Service
5301 Shawnee Rd
Alexandria, VA 22312

Telephone: (800) 553-6847
Facsimile: (703) 605-6900
E-Mail: orders@ntis.gov
Online order: https://classic.ntis.gov/help/order-methods/

ABSTRACT

This report investigates the integration of infrasound and seismic data to improve event localization accuracy, specifically focusing on a surface explosion at the Utah Training and Testing Range (UTTR). Utilizing the Seismoacoustic Bayesian Event Locator (SABEL) framework, we incorporated atmospheric specifications derived from Ground to Space (G2S) profiles to enhance celerity-range priors. Our analysis revealed that while the combination of infrasound and seismic observations significantly reduced localization uncertainty, challenges remained, particularly with returns at distances less than 200 km from the source and the influence of specific observations on location estimates. The results indicate that broader celerity distributions, such as those from Blom et al. (2020), facilitate better alignment with ground truth locations compared to narrower models. Overall, this work demonstrates the promise of seismoacoustic approaches in refining event localization and highlights the need for further exploration of celerity-range models to ensure reliable outcomes.

ACKNOWLEDGEMENTS

Sandia National Laboratories is a multimission laboratory managed and operated by National Technology & Engineering Solutions of Sandia, LLC, a wholly owned subsidiary of Honeywell International Inc., for the U.S. Department of Energy's National Nuclear Security Administration under contract DE-NA0003525.

This Low Yield Nuclear Monitoring (LYNM) research was funded by the National Nuclear Security Administration, Defense Nuclear Nonproliferation Research and Development (NNSA DNN R&D). The authors acknowledge important interdisciplinary collaboration with scientists and engineers from LANL, LLNL, NNSS, PNNL, and SNL.

SandiaAI was used in the preparation of this report.

CONTENTS

LIST OF FIGURES

LIST OF TABLES

This page left blank

ACRONYMS AND TERMS

Acronym/Term	Definition
BISL	Bayesian Infrasonic Source Location
EOF	Empirical Orthogonal Function
G2S	Ground-to-Space
GCA	Ground-Coupled Airwave
GMM	Gaussian Mixture Model
GT	Ground Truth
SABEL	Seismoacoustic Bayesian Event Locator
UTTR	Utah Test and Training Range

1. INTRODUCTION

Incorporating infrasound and seismic data has been shown to reduce uncertainty in location estimates (Koch and Arrowsmith 2019, Koch et al., 2024). Infrasound arrival times are not commonly used for event localization due to their larger uncertainties and, from array data, availability of comparatively low uncertainties from backazimuths. However, backazimuths cannot be obtained from single-station infrasound sensors, which are prevalent in shorter-term deployments due to their ease of use and lower cost (Busby and Aderhold, 2020).

Previous advances in infrasound localization methods include the development of a Bayesian infrasonic source location (BISL) algorithm, which determines event location and confidence intervals using infrasound arrival times and backazimuths (Modrak et al 2010). This work treated infrasound phases as unknown and formulated infrasound celerities as a uniform prior distribution between 0.28 and 0.34 km/s. Infrasound celerity is defined as the distance between the event and observation divided by travel time. Blom et al. (2015) improved on the BISL framework by expanding on the celerity prior to incorporate results from propagation modeling through atmospheric specifications. This work demonstrated the benefit of incorporating atmospheric models for regional scale infrasound observations. Recently, Blom et al. (2023) used empirical orthogonal functions to quantify spatial and seasonal trends in atmospheric structure using a suite of atmospheric profiles. This approach allows for a more accurate representation of uncertainty in propagation modeling while reducing computational costs.

To illustrate the concept of seismoacoustic localization, Koch and Arrowsmith (2019) developed the Seismoacoustic Bayesian Event Locator (SABEL) algorithm, building on the BISL framework. Their work showed that combining infrasound backazimuths and seismic arrival times can yield more precise event locations than either data type alone. Subsequently, Koch et al. (2024) expanded SABEL to include infrasound arrival times, demonstrating that even without infrasound arrays (and thus backazimuths), the integration of infrasound and seismic observations can significantly reduce uncertainty compared to using either data type independently. They also demonstrated the ability to use ground-coupled airwaves (GCA) recorded on seismic instruments as proxies for infrasound arrivals (Koch et al., 2024).

The objective of this study is to integrate the celerity-range priors developed by Blom et al. (2015) and Blom et al. (2023) into the SABEL framework (Koch and Arrowsmith, 2019; Koch et al., 2024). This integration aims to demonstrate the benefits of incorporating atmospheric specifications into seismoacoustic solutions, with the expectation that atmospheric models will enhance infrasound localization estimates, thereby improving overall seismoacoustic solutions. While this study primarily focuses on arrival times, the framework also allows for the inclusion of backazimuths, which would further enhance localization accuracy.

2. METHODS

2.1. SABEL: Seismoacoustic Bayesian Event Locator

SABEL is a Python package designed for the joint localization of seismic and infrasound events using a grid search algorithm. This package leverages the complementary nature of seismic and infrasound observations to reduce event location uncertainty. The grid search algorithm implemented in SABEL employs Bayesian inference principles to produce realistic uncertainty intervals based on the observed data (Koch and Arrowsmith, 2019 and Koch et al., 2024).

2.2. Input Data

SABEL uses two types of observations: arrival times and backazimuths. Both types can be obtained from seismic or infrasound instrumentation, but their corresponding uncertainties differ significantly. Generally, seismic data provides accurate arrival times, with pick uncertainties typically ranging from 0.1 to 1 second. In contrast, infrasound arrival times can exhibit emergent characteristics, leading to pick uncertainties of up to hundreds of seconds. Model uncertainties also vary; seismic velocities, even for simple 1-D models like AK135 (Kennett et al., 1995), are relatively stable due to the consistent velocity structure of the Earth over short time scales (Ballard et al., 2012). Conversely, infrasound model uncertainties arise from unpredictable variations in atmospheric structure, resulting in much larger uncertainties. Backazimuths exhibit an opposite trend: infrasound arrays yield relatively low uncertainties for backazimuths (Nippress and Green, 2023), while seismic azimuths from 3-component sensors can be highly uncertain due to local heterogeneities in Earth's structure (Noda et al., 2012).

2.2.1. Arrival Times

2.2.1.1. Seismic

Here we briefly describe the methodology used for the seismic arrival times. The methodology for seismic arrival times uses the AK135 (Kennet et al., 1995) velocity model to calculate the predicted seismic arrival time for each event hypothesis (φ, λ, t) at the observation point (d). Where φ and λ are latitude and longitude, t is the origin time. We assume a surface explosion and use a fixed depth of 0. Residuals are computed between each observation and every event hypothesis. These residuals, *r,* are then transformed into a likelihood assuming a Gaussian distribution (Eq. 1):

Eq 1. $$gauss = \frac{1}{\sqrt{2\pi\sigma^2}} exp\left(-\frac{r^2}{2\sigma^2}\right)$$

Where σ represents the combined model and pick uncertainties. This provides the individual likelihood function for a single observation, and once all individual likelihood functions are constructed, they are multiplied together to form a joint likelihood function.

2.2.1.2. Infrasound

Previous work by Koch et al. (2024) followed the same approach as in section 2.2.1.1 and explored different model uncertainty functions for a constant celerity forward model. Here, we follow the approach of Blom et al. (2015) to incorporate prior estimates of celerity likelihood and expand beyond a single, constant celerity forward model. We employ ground-to-space (G2S) atmospheric specifications (Hetzer et al., 2019) for the region surrounding the expected event location. To account for model uncertainty, we introduce perturbations to these profiles using empirical orthogonal function analysis, as outlined in Blom et al. (2023) and detailed in Section 3.

Unlike the forward model approach in Section 2.2.1.1 and previous work by Koch et al. (2024), this method does not assume a forward model. Instead, we calculate the celerity and distance between each event hypothesis and observation. The likelihood for an individual event hypothesis is then determined using prior estimates of celerity, which can be distance dependent or distance independent. This is done for all event hypothesis in the grid space to form the individual likelihood function. Construction of these celerity priors is explained in the following section. For a single infrasound arrival, this is equivalent to the individual likelihood function, which can be combined with other individual likelihood functions by multiplying them together to form a joint likelihood function. We incorporate pick uncertainty by calculating the celerity that would result from either end of the pick uncertainty and averaging those values.

2.2.1.3. Data Fusion

The joint likelihood from each approach (seismic and infrasound) can be combined by multiplying them together. The resulting distribution is then normalized over the model space to form a posterior distribution and marginalized to return spatial and temporal confidence intervals.

3. DATA

This study uses a surface explosion resulting from the explosive disposal of old rocket motors at the Utah Test and Training Range (UTTR) on August 1st, 2007. This event produced detectable infrasound arrivals over 400 km away. The same event was previously included in a study by Park et al., 2017 where they used infrasound arrivals on seismic sensors for detection and localization. An expert analyst picked both seismic and infrasound arrival times, focusing on the first arrival time. The observations include infrasound arrivals at 27 stations (including individual elements at arrays), 123 GCA recorded on seismometers, and 57 Pg or Pn arrivals on seismic sensors. Based on the seismic data, the analyst determined an origin location of longitude -112.917 and latitude 41.128, with an origin time of 20:01:24 UTC. Although we lack the absolute ground truth (GT) for this event, the extensive seismic observations provide sufficient coverage to treat the analyst's seismic-only location and origin time as a pseudo-GT, which we refer from this point onwards as GT.

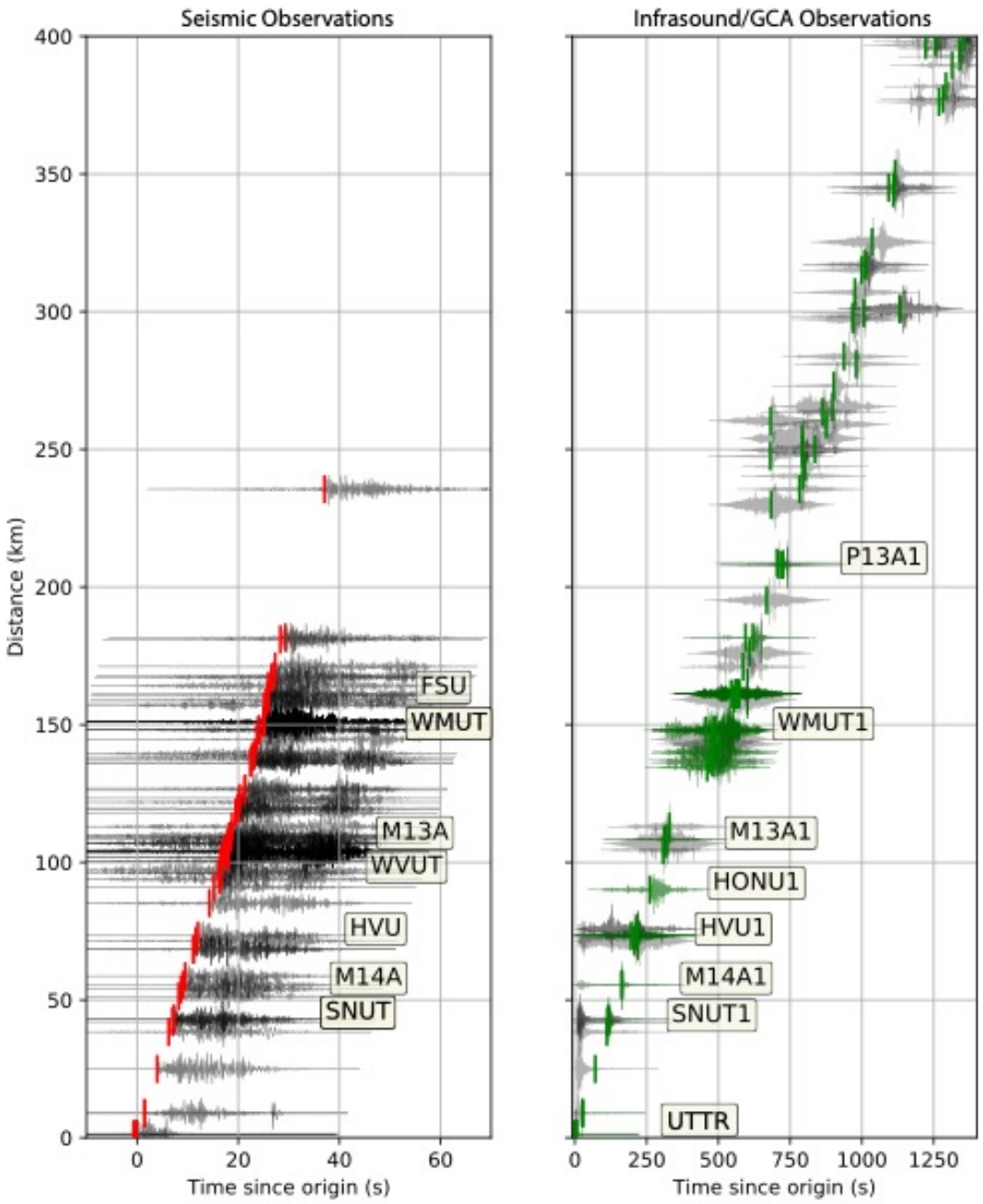

Figure 3-1 (A) Seismic and (B) acoustic record sections showing analyst picks. Record sections are built using the GT time and location. Black waveforms represent signals recorded on seismic instruments, and green waveforms represent signals recorded by infrasound instruments. Red lines are Pg and Pn arrivals, and green lines are infrasound arrivals. Labeled stations are those using the "subset" of arrivals.

G2S atmospheric specifications were downloaded between July 15th and August 15th at 20:00 each day between 2005 and 2024, resulting in 402 profiles, in to capture potential atmospheric variability (Hetzer et al., 2019). Following the procedure outlined in Blom et al. (2023), we compute the empirical orthogonal functions (EOFs) to form the suite of atmospheric profiles, calculate the coefficients of the EOFs, and use these coefficients to reconstruct profiles. We found that using 70

coefficients was sufficient to accurately reproduce the observed variations. Next, using the atmospheric specification for the GT time and location, we construct perturbations to the specification using the EOFs, 70 coefficients, and a standard deviation of 5. The resulting profiles are shown in Figure 3-2. Finally, we run propagation modeling using infraGA on each of the resulting profiles. The propagation modeling is conducted with the GT location as the source, inclinations from 0 to 45° with a step size of 1°, and azimuths from 0 to 360° with a step size of 2°. Figure 3-3 shows the resulting bounce points. A 2-D Gaussian mixture model is then used to fit the resulting celerity-range distribution of each bounce point (Figure 3-4) using sklearn's BayesianGaussianMixture tool (Pedregosa et al., 2011).

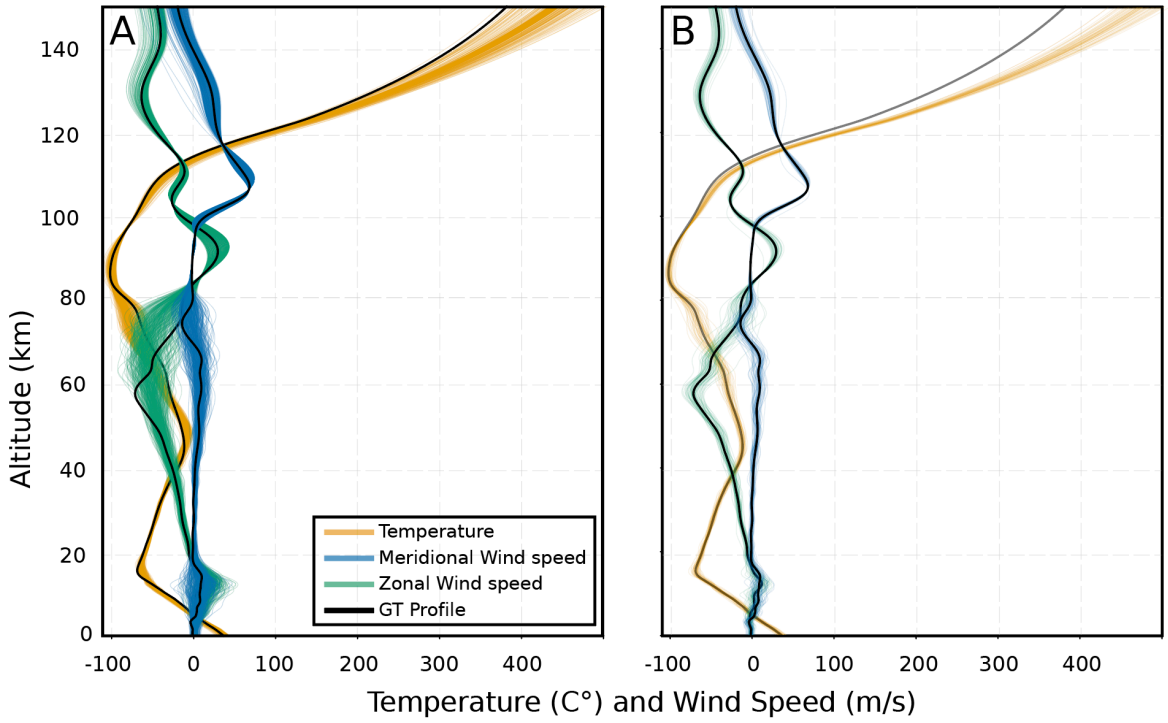

Figure 3-2 A) G2S atmospheric specifications between 2005-2024 for July 15 – August 15 at 20:00 UTC. B) Stochprop representative profiles calculated using 70 coefficients.

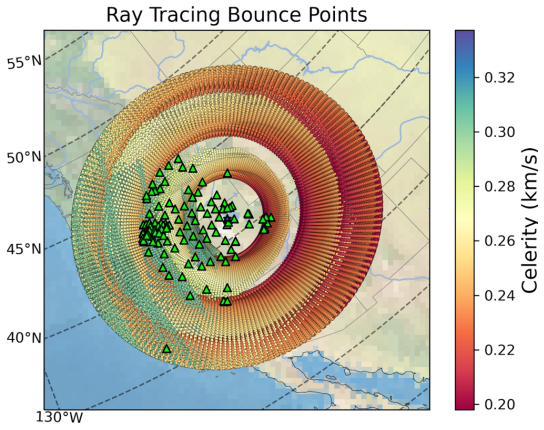

Figure 3-3 Bounce points from propagation modelling.

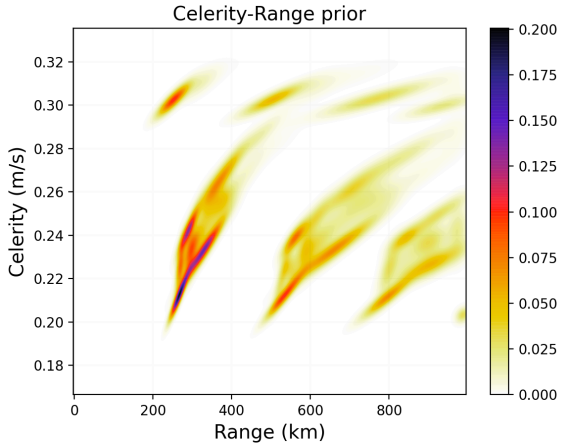

Figure 3-4 Celerity range prior distribution. The color bar is the likelihood.

In addition to the propagation modeling-informed celerity-range priors, we also explore using range-independent priors (Figure 3-5). We include the model from Blom et al. (2020), which used propagation modeling for 6 years of G2S data to determine the distribution of celerity models. Additionally, we incorporate an atmospheric celerity model from Nippress and Green (2023), which was formed using detections from ground truth events recorded on the International Monitoring System's Infrasound network to determine celerity distributions.

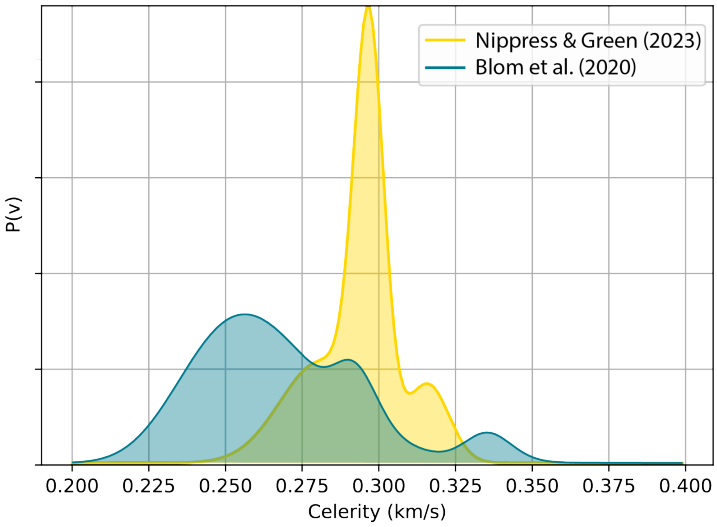

Figure 3-5 Range independent celerity distributions.

4. RESULTS

Using the celerity models described in the previous section, we relocate the observations for the UTTR explosion. Table 1 summarizes results from localizations using all different models and observations. Initially, locations were calculated using the full suite of infrasound arrivals. The Gaussian Mixture Model (GMM; Table 1) celerity-range model resulted in no maximum likelihood. When using the range-independent distributions, both models placed the location far from the GT location, and neither contained the origin time nor location in their confidence intervals.

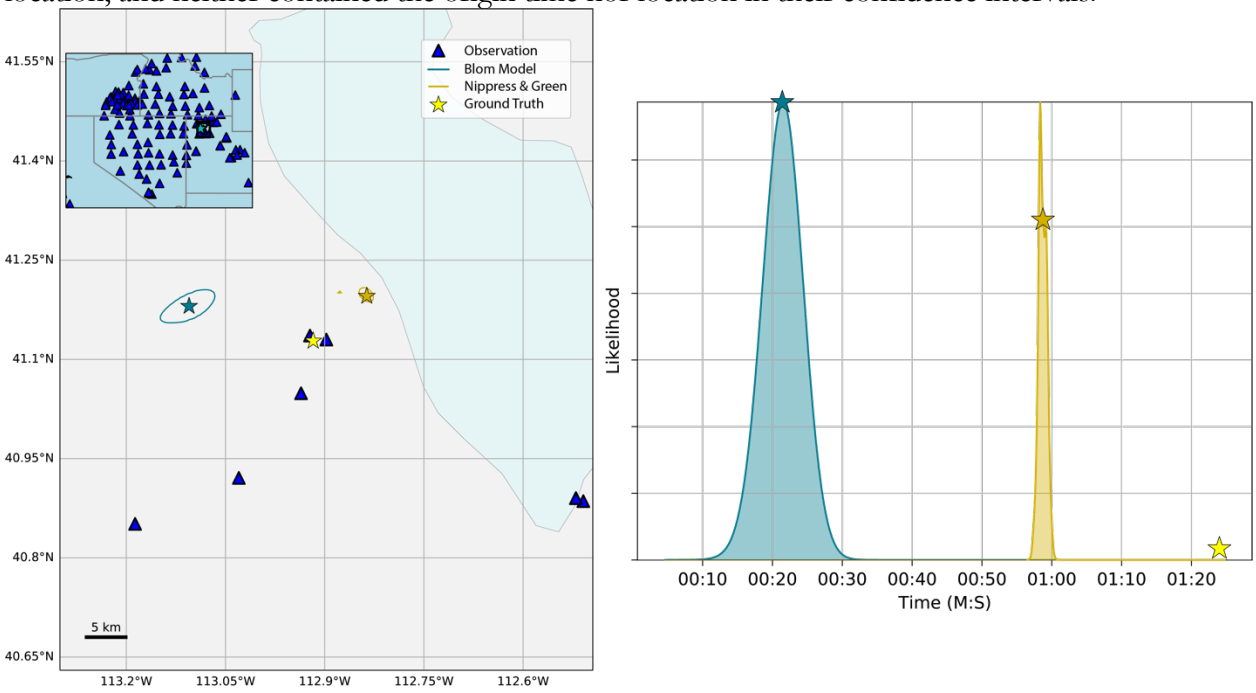

Figure 4-1 Spatial (left) and temporal (right) distributions using all infrasound arrivals. Contours are the 95% confidence interval. Stars represent maximum likelihood of the different models and the GT location (Yellow).

To better understand this behavior, we took a subset of infrasound arrivals, keeping only those recorded at infrasound stations, and only using a single observation from arrays of instruments. This decimates the observations to 8. When using this subset, all locations are improved, but as before, the seismic GT is not contained in any confidence interval (Figure 4-2).

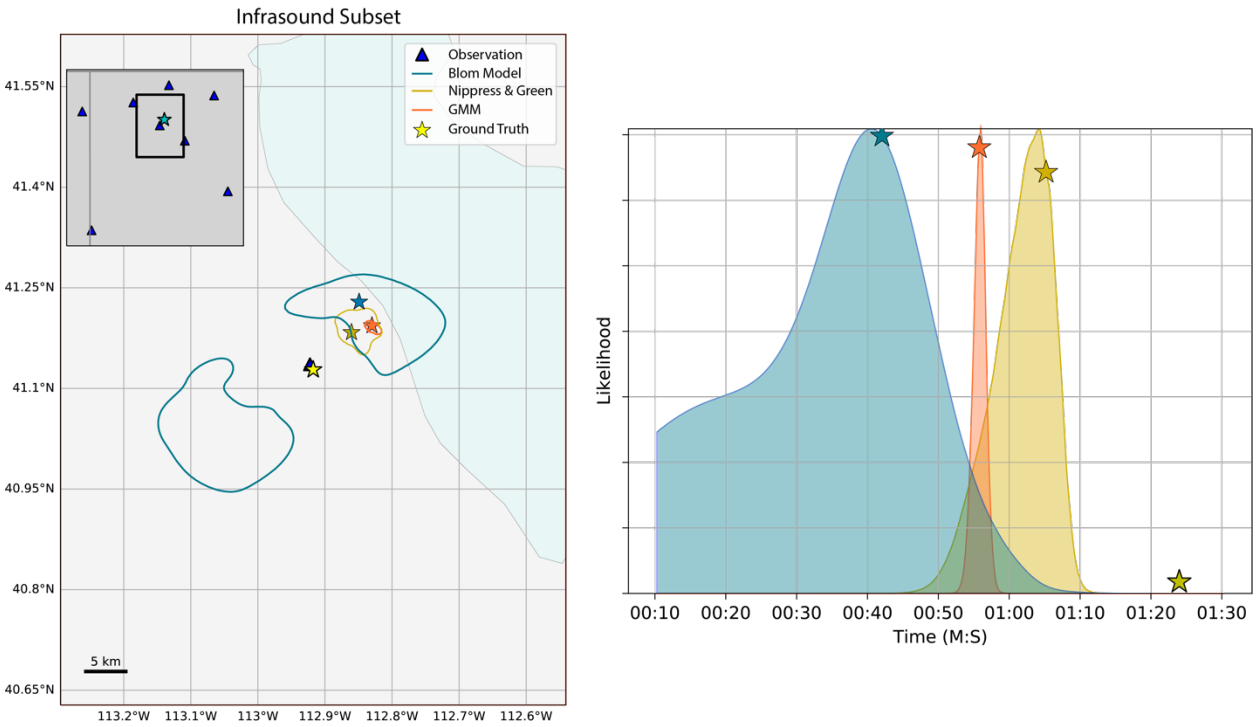

Figure 4-2 Spatial (left) and temporal (right) distributions using subset of infrasound arrivals.

When examining these distributions, it seems evident the signal recorded at the closest acoustic station, UTTR, is inconsistent with a very-local source. The Blom et al. (2020) prior in particular shows a bimodal distribution with a gap surrounding the UTTR station. Removing the UTTR observation, the locations improve significantly. All models now locate the GT location in the 95% interval (Figure 4-3). However, the origin time is still not included in any of the confidence intervals.

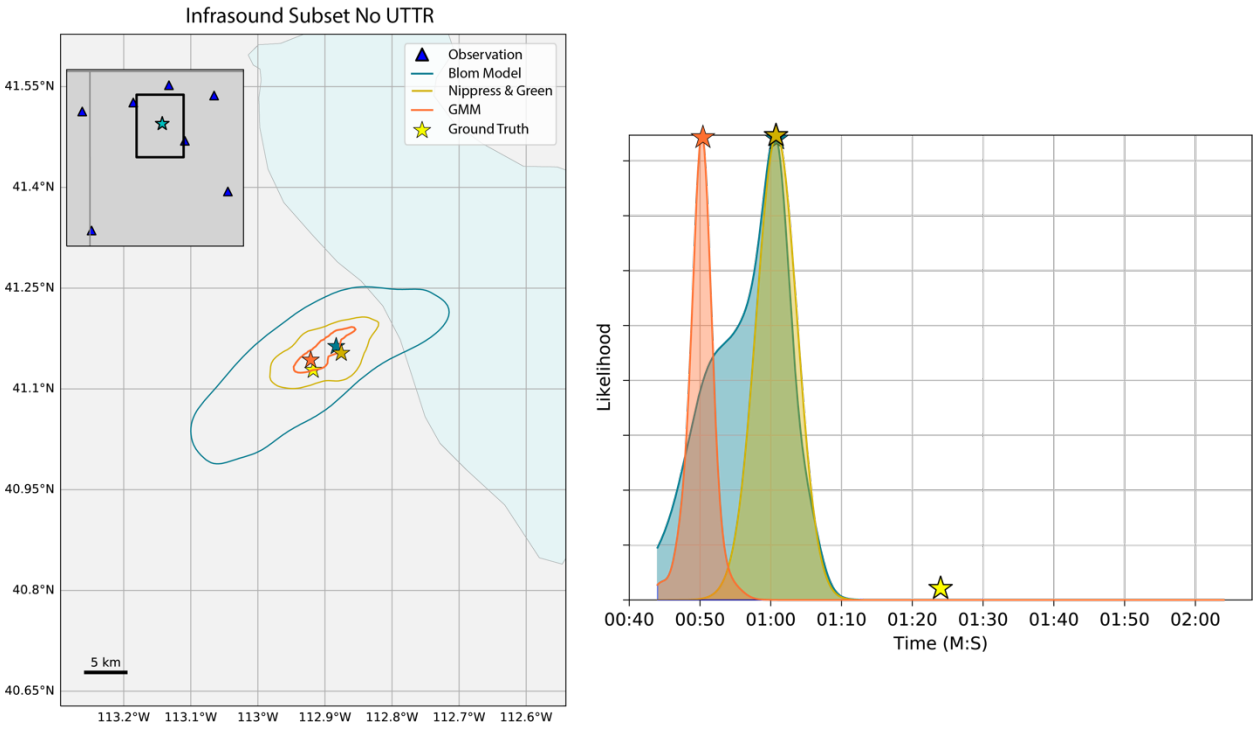

Figure 4-3 Spatial (left) and temporal (right) distributions using the subset of infrasound arrivals with the UTTR observation removed.

Finally, we explore the seismoacoustic solution. To ensure both the infrasound and seismic observations are represented equally, we subset the seismic observations, keeping only the closest observations to the remaining infrasound observations. Figure 4-4 shows the resulting seismic-only location. Both location and origin time are within the confidence interval. The full seismoacoustic solution shows a significant reduction in uncertainty in comparison to the seismic only solution (Figure 4-5). However, this comes at the expense of accuracy. The GMM fails to contain either the origin time or location. The range independent model based on Nippress and Green (2023) fails to contain the location. The Blom et al. (2020) model, however, manages to accurately locate both origin time and location and reduces uncertainty by ~92%.

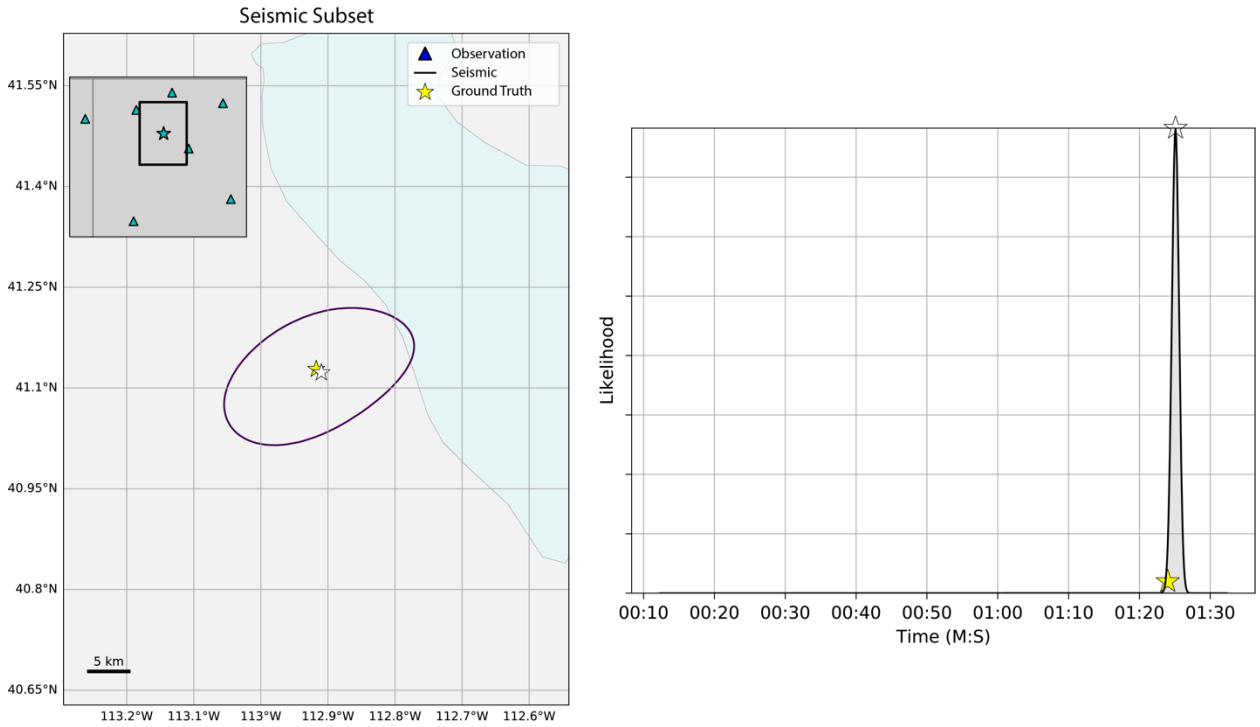

Figure 4-4 Spatial (left) and temporal (right) distributions using a subset of seismic observations.

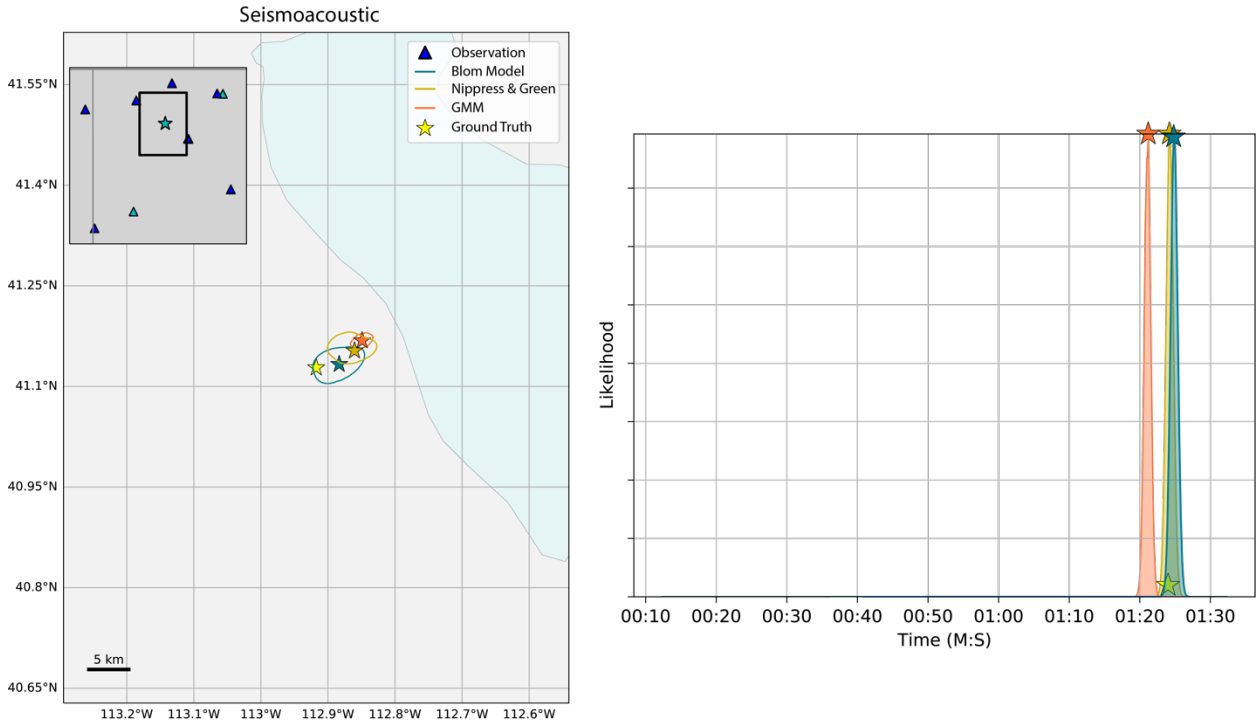

Figure 4-5 Spatial (left) and temporal (right) distributions using seismoacoustic observations. Both infrasound and seismic arrivals are the subset of arrivals without UTTR.

Table 1 Results of location using different observations and models.

Input data	Model	GT location in 95%	GT Time in 95 %	Uncertainty Size	
				Area (sq km)	Time (s)
All Infra	GMM	FALSE	FALSE	-	-
	Nipppress & Green	FALSE	FALSE	3.16	6.317
	Blom (2020)	FALSE	FALSE	23.66	11.529
Infra Subset	GMM	FALSE	FALSE	3.05	3.5
	Nippress & Green	FALSE	FALSE	30.4	15.539
	Blom (2020)	FALSE	FALSE	411.12	44.812
No UTTR	GMM	TRUE	FALSE	22.18	7.92
	Nippress & Green	TRUE	FALSE	100.58	19.95
	Blom (2020)	TRUE	FALSE	479.49	51.889
Seismic	Ak135	TRUE	TRUE	375.99	2.005
SA	GMM	FALSE	FALSE	5.41	1.805
	Nippress & Green	FALSE	TRUE	23.69	2.005
	Blom (2020)	TRUE	TRUE	28.89	1.905

5. DISCUSSION

The propagation modeling produced no infrasound arrivals at distances < 200 km (Figure 3-4). The continuous infrasound and GCA arrivals observed for this event suggest that the atmospheric profiles used in the propagation modeling failed to capture important variability, which can cause returns at these distances. The lack of returns at distances < 200 km is likely the reason the Gaussian Mixture Model (GMM) struggled to accurately locate the explosion. Using all arrivals, far too many observations would have had very low likelihoods of an event occurring within this range; combining so many low likelihoods failed to produce any maximum within the grid range. By using the subset of observations, all but one observation fell within this 200 km range. Further testing is needed to fully understand the behavior of the likelihood function in this regime. Dannemann Dugick et al. (2020) evaluated the BISL location method on a variety of UTTR surface explosions and found similar results when using seasonally representative celerity-range distributions.

The UTTR acoustic station's observation has a celerity of approximately 124 m/s using the seismic GT location. This is outside the range used in the celerity priors, so it is not surprising that including this observation pushed the location further away. It is unclear why this observation has such a slow celerity, it may be complicated pathing due to local topography, or it could be a picking timing error in the GT that is influencing the interpretation. A full understanding of this will require a deeper exploration of this specific observation.

When comparing the range-independent prior models from Blom et al. (2020) and Nippress and Green (2024), the Blom model has a wider distribution that accounts for tropospheric, thermospheric, and stratospheric arrivals. Although the thermospheric arrivals have the highest weighting, the broad distribution still supports observations at faster celerities. In contrast, the Nippress and Green model is comparatively narrow, even if the peak of the distribution is more consistent with the expected arrivals at local to regional distances. When combined with the seismic observations, the broadness of the Blom et al. (2020) distribution is what allows for the GT to be contained within the confidence interval.

The large reduction in uncertainty we observe when including infrasound arrivals is promising. However more work is needed to fully understand the reliability of different celerity-range models.

6. CONCLUSIONS

This report highlights the potential of integrating infrasound and seismic data to enhance event localization accuracy. Using a SABEL coupled with prior estimates of celerity distributions informed by atmospheric specifications we demonstrate that the combination of these data types can substantially reduce uncertainty in locating events like the UTTR explosion. Despite challenges, such as the lack of returns at shorter distances and the influence of specific observations on location estimates, our findings underscore the importance of refining celerity-range models. Future work will focus on further understanding the reliability of these models and optimizing the integration of atmospheric data to improve event localization.

REFERENCES

[1] Ballard, S., Hipp, J. R., Begnaud, M. L., Young, C. J., Encarnacao, A. V., Chael, E. P., & Phillips, W. S. (2016). SALSA3D: A tomographic model of compressional wave slowness in the Earth's mantle for improved travel-time prediction and travel-time prediction uncertainty. *Bulletin of the Seismological Society of America*, *106*(6), 2900-2916.

[2] Blom, P. S., Marcillo, O., & Arrowsmith, S. J. (2015). Improved Bayesian infrasonic source localization for regional infrasound. *Geophysical Supplements to the Monthly Notices of the Royal Astronomical Society*, *203*(3), 1682-1693.

[3] Blom, P., Euler, G., Marcillo, O., & Dannemann Dugick, F. (2020). Evaluation of a pair-based, joint-likelihood association approach for regional infrasound event identification. *Geophysical Journal International*, *221*(3), 1750-1764.

[4] Blom, P., Waxler, R., & Frazier, G. (2023). Quantification of spatial and seasonal trends in the atmosphere and construction of statistical models for infrasonic propagation. *Geophysical Journal International*, *235*(2), 1007-1020.

[5] Busby, R. W., & Aderhold, K. (2020). The Alaska transportable array: As built. *Seismological Research Letters*, *91*(6), 3017-3027.

[6] Dannemann Dugick, F. K., Blom, P. S., Stump, B. W., Hayward, C. T., Arrowsmith, S. J., Carmichael, J. C., & Marcillo, O. E. (2022). Evaluating the location capabilities of a regional infrasonic network in Utah, US, using both ray tracing-derived and empirical-derived celerity-range and backazimuth models. *Geophysical Journal International*, *229*(3), 2133-2146.

[7] Hetzer, C.H., Drob, D.P., and Zabel, K. (2019). The NCPA-G2S request system. https://g2s.ncpa.olemiss.edu. Accessed 2024-09-01.

[8] Kennett, B. L., Engdahl, E. R., & Buland, R. (1995). Constraints on seismic velocities in the Earth from traveltimes. *Geophysical Journal International*, *122*(1), 108-124.

[9] Koch, C. D., & Arrowsmith, S. (2019). Locating surface explosions by combining seismic and infrasound data. *Seismological Research Letters*, *90*(4), 1619-1626.

[10] Koch, C., Berg, E. M., Dannemann Dugick, F. K., Albert, S., & Brogan, R. (2024). *Event Location using Arrival Times from Seismic and Acoustic Phenomena* (No. SAND2024-00821). Sandia National Lab.(SNL-NM), Albuquerque, NM (United States).

[11] Modrak, Ryan T., Stephen J. Arrowsmith, and Dale N. Anderson. "A Bayesian framework for infrasound location." *Geophysical Journal International* 181, no. 1 (2010): 399-405.

[12] Nippress, A., & Green, D. N. (2023). Global empirical models for infrasonic celerity and backazimuth. *Geophysical Journal International*, *235*(2), 1912-1925.

[13] Noda, S., Yamamoto, S., Sato, S., Iwata, N., Korenaga, M., & Ashiya, K. (2012). Improvement of back-azimuth estimation in real-time by using a single station record. *Earth, planets and space*, *64*, 305-308.

DISTRIBUTION

Email—Internal

Name	Org.	Sandia Email Address
Clinton Koch	6756	clikoch@sandia.gov
Fransiska Dannemann-Dugick		fkdanne@sandia.gov
Elizabeth Berg	6756	eliberg@sandia.gov
Sarah Albert	6752	salber@sandia.gov
Technical Library	1911	sanddocs@sandia.gov

Email—External

Name	Company Email Address	Company Name
John Lazarz	john.lazarz@nnsa.doe.gov	NNSA DOE
Rengin Gok	m.rengin.gok@nnsa.doe.gov	NNSA DOE

Hardcopy—Internal

Number of Copies	Name	Org.	Mailstop

Hardcopy—External

Number of Copies	Name	Company Name and Company Mailing Address

This page left blank

Sandia National Laboratories

Sandia National Laboratories is a multimission laboratory managed and operated by National Technology & Engineering Solutions of Sandia LLC, a wholly owned subsidiary of Honeywell International Inc. for the U.S. Department of Energy's National Nuclear Security Administration under contract DE-NA0003525.